ACS APPLIED MATERIALS & INTERFACES

Research Article

www.acsami.org

Sulfur Nanogranular Film-Coated Three-Dimensional Graphene Sponge-Based High Power Lithium Sulfur Battery

Wook Ahn, Min Ho Seo, Yun-Seok Jun, Dong Un Lee, Fathy M. Hassan, Xiaolei Wang, Aiping Yu, and Zhongwei Chen*

Department of Chemical Engineering, University of Waterloo, 200 University Avenue West Waterloo, Ontario N2L3G1, Canada

Supporting Information

ABSTRACT: To meet the requirements of both high energy and power density with cycle durability of modern EVs, we prepared a novel nanosulfur granular assembled film coated on the three-dimensional graphene sponge (3D-GS) composite as a high-performance active material for rechargeable lithium sulfur batteries. Instead of conventional graphene powder, three-dimensional rGO sponge (3D-rGO) is employed for the composite synthesis, resulting in a sulfur film directly in contact with the underlying graphene layer. This significantly improves the overall electrical conductivity, strategically addressing challenges of conventional composites of low sulfur utilization and dissolution of polysulfides. Additionally, the synthesis mechanism of 3D-GS is elucidated by XPS and DFT analyses, where replacement of hydroxyl group of 3D-rGO sponge by sulfur (S_8) is found to be thermodynamically favorable. As expected, 3D-GS demonstrates outstanding discharge capacity of 1080 mAh g^{-1} at a 0.1*C* rate, and 86.2% capacity retention even after 500 cycles at a 1.0*C* rate.

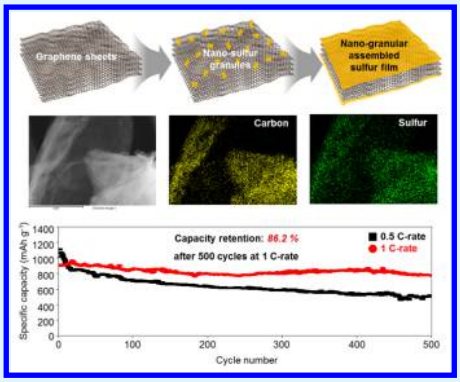

KEYWORDS: *lithium sulfur battery, nano sulfur granules assembled film, graphene sponge, three-dimensional graphene, sulfur-graphene composite*

INTRODUCTION

Recently, lithium-based rechargeable battery technologies have become the focal point of research to fulfill the requirements of electric vehicles (EVs), the most desired one being an extended driving range of 300−400 mile per full charge.[1,2] To meet these requirements, however, a breakthrough in current lithium-based rechargeable batteries is necessary.[3,4] Currently the most utilized and investigated lithium ion battery technology is capable of generating energy density up to 387 Wh kg^{-1}, which is significantly lower than other rechargeable batteries such as lithium sulfur and lithium air batteries.[5−7] Among many emerging battery technologies, rechargeable lithium sulfur batteries are thought of as one of the most promising candidates for addressing the needs of full-time EVs.[8,9] Particularly, lithium sulfur batteries based on sulfur−carbon composite electrodes utilizing carbon materials have been studied extensively.[8−10] The composite materials have been developed by combining sulfur with a homogeneously dispersed conductive carbon, reinforcing electrical conductivity, and preventing the dissolution of lithium polysulfide into the organic electrolyte.[11−13] These enhancements of active sulfur−carbon composites in turn significantly improve the material utilization during the charge−discharge cycling process.[14−16] Particularly, graphene-based sulfur−carbon composites prepared by various chemical reaction routes have been shown to demonstrate high *C*-rate capability,[17−19] which is very interesting for EV applications. Until now, the most reported work related to the morphology of graphene based sulfur−carbon composites has been limited to aggregated particles of sulfur either dispersed in the graphene matrix or wrapped by graphene sheets.[18,20,21] Furthermore, a novel binder-free sulfur-graphene composite has been reported, which consists of free-standing porous and interconnected 3D network of graphene foam, for lithium sulfur battery applications.[5,20,22] Additionally, an in-depth study with emphasis on revealing the reaction mechanism during sulfur−carbon composite formation has never been reported for further investigation on cathode materials using 3D graphene sponge.

Herein, we introduce a film consisting of an assembly of tiny sulfur nanogranules coated on the three-dimensional graphene sponge, where the final composite morphology is a uniform sulfur film laminated over the surface of graphene sheets. Additionally, theoretical calculation of possible reaction model of sulfur and graphene was conducted to prove the reaction mechanism for the generation of sulfur nanofilm laminated on the graphene sheets. The following advantages of the sulfur-graphene composite as the active material for the solution of lithium sulfur battery are as follows: (i) the direct connection between sulfur film and the underlying graphene layer significantly improves intrinsically low electrical conductivity of sulfur; (ii) highly aligned three-dimensional graphene sponge structure minimizes the dissolution of sulfur by chemical

Received: October 26, 2015
Accepted: January 8, 2016
Published: January 8, 2016

DOI: 10.1021/acsami.5b10267
ACS Appl. Mater. Interfaces 2016, 8, 1984−1991

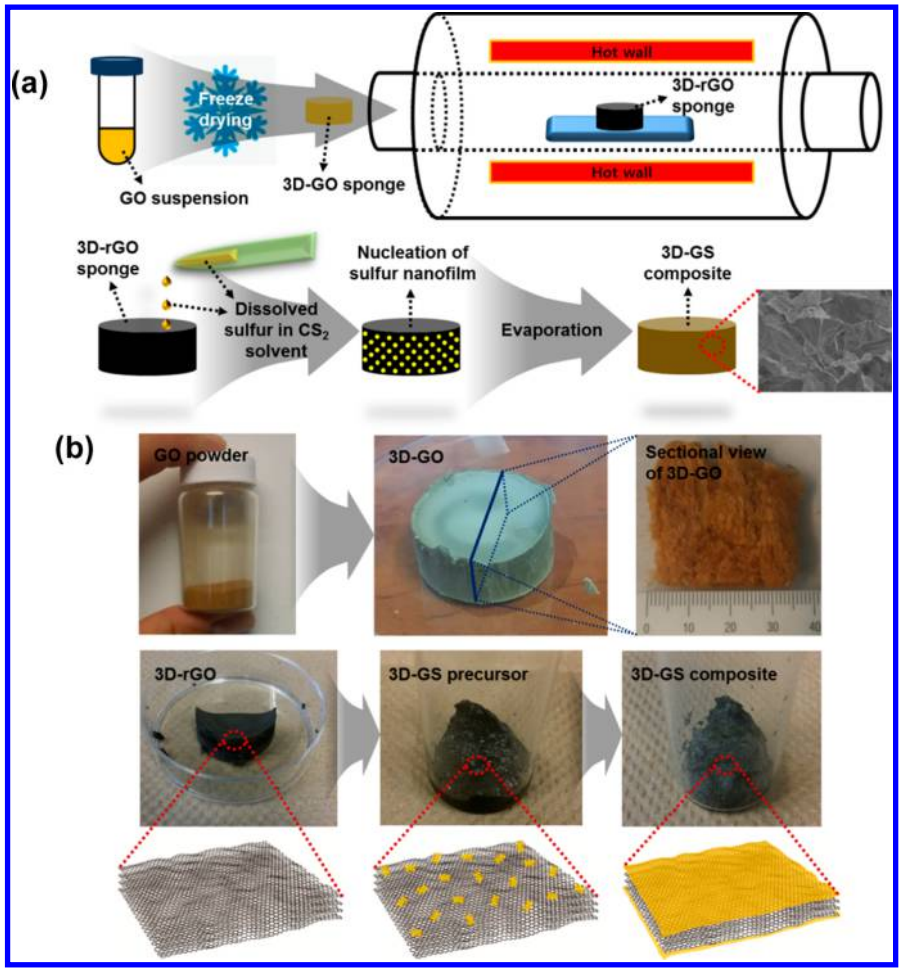

Figure 1. Schematic synthesis procedure of 3D structured sulfur-rGO sponge (3D-GS) composite. (a) Unique nanogranules assembled 3D-GS composite prepared by a facile low-temperature solution method using carbon disulfide (CS_2) as solvent. (b) Optical observations at each stage of 3D-GS synthesis.

bonding during charge−discharge cycling; (iii) the unique sulfur-graphene composite morphology leads to high power due to excellent *C* rate capability in addition to high energy capacity and its retention, which are particularly interesting for high performance EV applications.

RESULTS AND DISCUSSIONS

The schematic illustration of the synthesis process of sulfur-rGO sponge composite (3D-GS) is presented in Figure 1a. The sponge structure has been maintained throughout the solution-based synthesis procedure, and the three-dimensionally structured graphene sponge plays the role of electrically conductive matrix by direct contacting with sulfur film for improved material utilization.

We refer to the prepared materials as 3D-GO (graphite oxide sponge), 3D-rGO (reduced graphene oxide sponge), and 3D-GS (sulfur-rGO sponge) composite. In order to compare the electrochemical properties, the mixture of sulfur with rGO by ball-milling, and the sulfur-rGO composite was also prepared and denoted as M-GS (sulfur-rGO mixture), and C-GS (sulfur-rGO composite), respectively. In order to quantify the amount of sulfur in the 3D-GS composite, the TG analysis has been carried out and the result is shown in the Figure S1, demonstrating approximately 74 wt % sulfur in the 3D-GS composite. The morphological change from 3D-rGO to 3D-GS after loading sulfur into the graphene sponge and related EDX elemental mapping of sulfur (Figures S2 and S3) shows very uniform distribution, and it is virtually identical to the carbon distribution, indicating that sulfur nano granules are very well dispersed throughout the surface of 3D-rGO.

The XRD patterns obtained with 3D-GS and 3D-rGO are consistent with results from the literature.[23] The further discussion is presented in Figure S4 and Table S1.

TEM analysis has been conducted, where the average particle size of graphene sheets (3D-rGO) is observed to be 1−2 μm as shown in Figure 2a, and the fringes observed in high-resolution TEM image (Figure 2b) is a clear indication that 3D-rGO has been successfully graphitized through the thermal reduction. However, the irregular dots observed are likely due to remaining oxygen functional groups ascribed from an incomplete reduction of rGO sheets. The sulfur nano granules assembled film laminated on the surface of rGO sponge after synthesis procedure is confirmed by no aggregated particles observed under HRTEM as shown in Figure 2c, d. Further analysis by STEM (Figure 2e) also shows that the sulfur film in 3D-GS is observed to exist as particle-free, continuously laminate layer. However, sulfur particles with an average size between 6−8 nm are observed in very limited areas, where the graphene sheets are folded or aggregated as shown in the STEM image of Figure 2f. To characterize the elemental distribution in this limited area shown in the STEM image, EDX mapping was carried out as shown in the Figure S6. On

DOI: 10.1021/acsami.5b10267
ACS Appl. Mater. Interfaces 2016, 8, 1984−1991

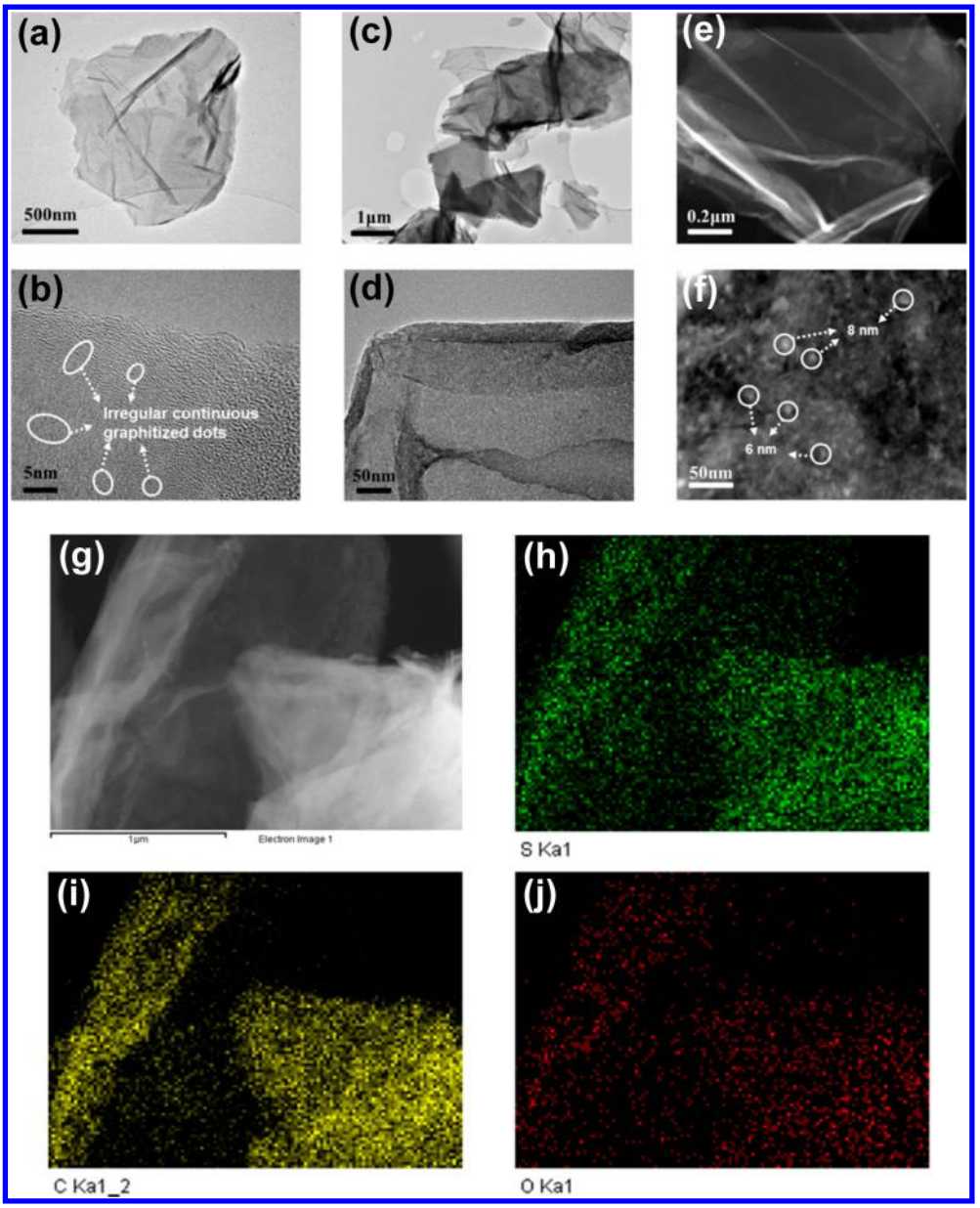

Figure 2. Morphological and elemental analysis by TEM and EDX of 3D-rGO and 3D-GS. (a) Typical wrinkled morphology of graphene sheets and (b) fingerprint fringes observed by HRTEM with 3D-rGO. (c, d) High-resolution of TEM image of 3D-GS. (e–g) High-resolution STEM image of 3D-GS and (h–j) its elemental mapping result.

the basis of very uniform distribution of sulfur that matches exactly with carbon and oxygen maps, it is most likely that the sulfur predominantly exists as tiny nanogranules that have assembled filmlike morphology. This result is a strong indication that the sulfur film is formed by a dense assembly of tiny nanogranules. The previous observations of the continuous sulfur film is most likely due to much smaller size of sulfur nanogranules assembled and coated on the surface of RGS, which may be difficult to be characterized by TEM. To further build on the observations of nano granules of sulfur, the film on the surface of rGO sponge, elemental mapping through EDX has been carried out. As shown in Figure 2g–j, virtually exact replicas of sulfur, and carbon maps obtained verifies that the sulfur distribution extremely uniform. The observed oxygen distribution is indicative of remaining oxygen functional groups after sulfur deposition.

For three-dimensional Raman mapping of 3D-GS, an island of graphene sheet surrounded by the voids of graphene sponge has been carefully selected as shown in the Figure 3a, where white to blue color gradient corresponds to high to low concentration of sulfur, respectively. The Raman spectra obtained across the map and into the depth of 3D-GS are presented in Figure S7, clearly illustrating the existence of voids surrounding a continuous sulfur film laminated on the rGO sheet. The Raman spectrum obtained from 4 levels of 3D-GS with each level being 1 μm in thickness (total depth of 4 μm) and consisting of 25 in-plane measurements clearly indicates the existence of sulfur (Figure 3b). Figure 3c, d show typical Raman spectra of 3D-GS composite showing peaks that correspond to D, G and 2D-band peaks of graphene and sulfur, respectively.[24,25] In particular, relatively high intensity of the D-band peak is ascribed to the defects of graphene layer (I_D/I_G = 1.32), which supports previously observed irregular

DOI: 10.1021/acsami.5b10267
ACS Appl. Mater. Interfaces 2016, 8, 1984–1991

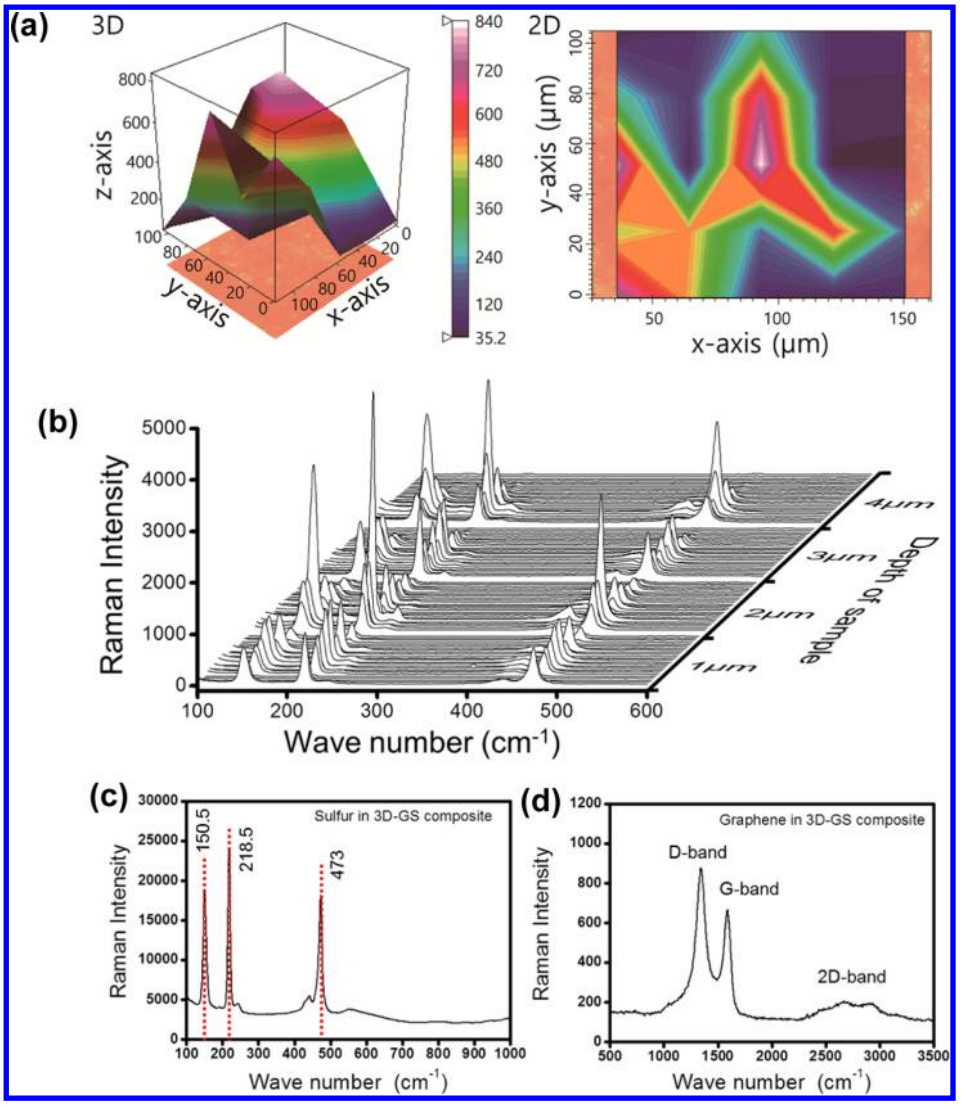

Figure 3. (a) Three- and two-dimensional Raman maps of 3D-GS composite obtained by (b) image processing of four levels of Raman measurements with each level being 1 μm in thickness (for the total depth of 4 μm) and consisting of 25 in-plane measurements. (c, d) Typical Raman spectra of graphene and sulfur obtained with 3D-GS composite.

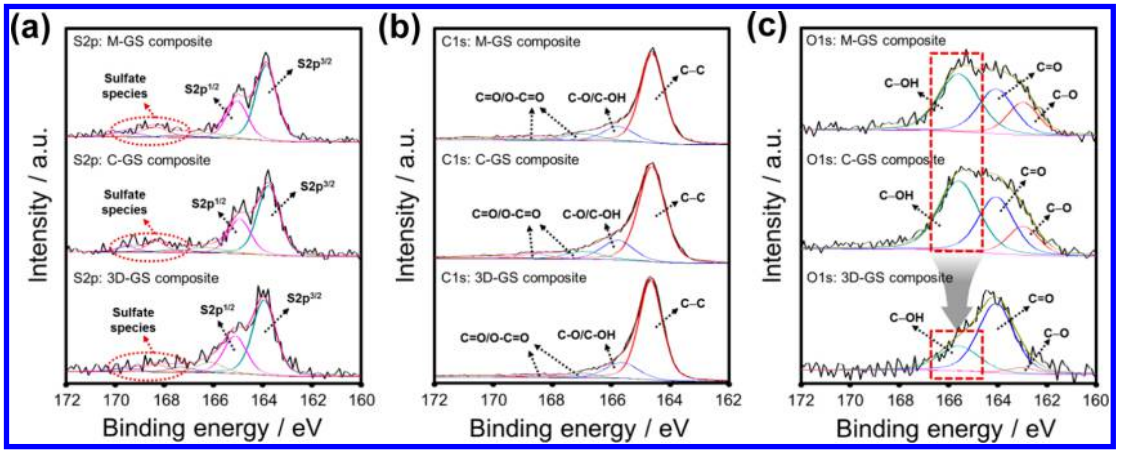

Figure 4. XPS analysis of S 2p, C 1s, and O 1s of M-GS, C-GS, and 3D-GS composites; (a) S 2p XPS spectra of M-GS, C-GS, and 3D-GS confirming the existence of elemental sulfur. (b) XPS results of C 1s of M-GS, C-GS, and 3D-GS. (c) Characteristic peaks of oxygen bonded carbon identified in O 1s are C−O, C═O, and C−O−H, which correspond to the reported binding energies of 530.9, 532.2, and 533.6 eV, respectively.

continuous graphitized carbon configuration in the high resolution TEM image.

The S 2p doublet peaks of M-GS, C-GS and 3D-GS presented in Figure 4a very closely matches with the previously

DOI: 10.1021/acsami.5b10267
ACS Appl. Mater. Interfaces 2016, 8, 1984−1991

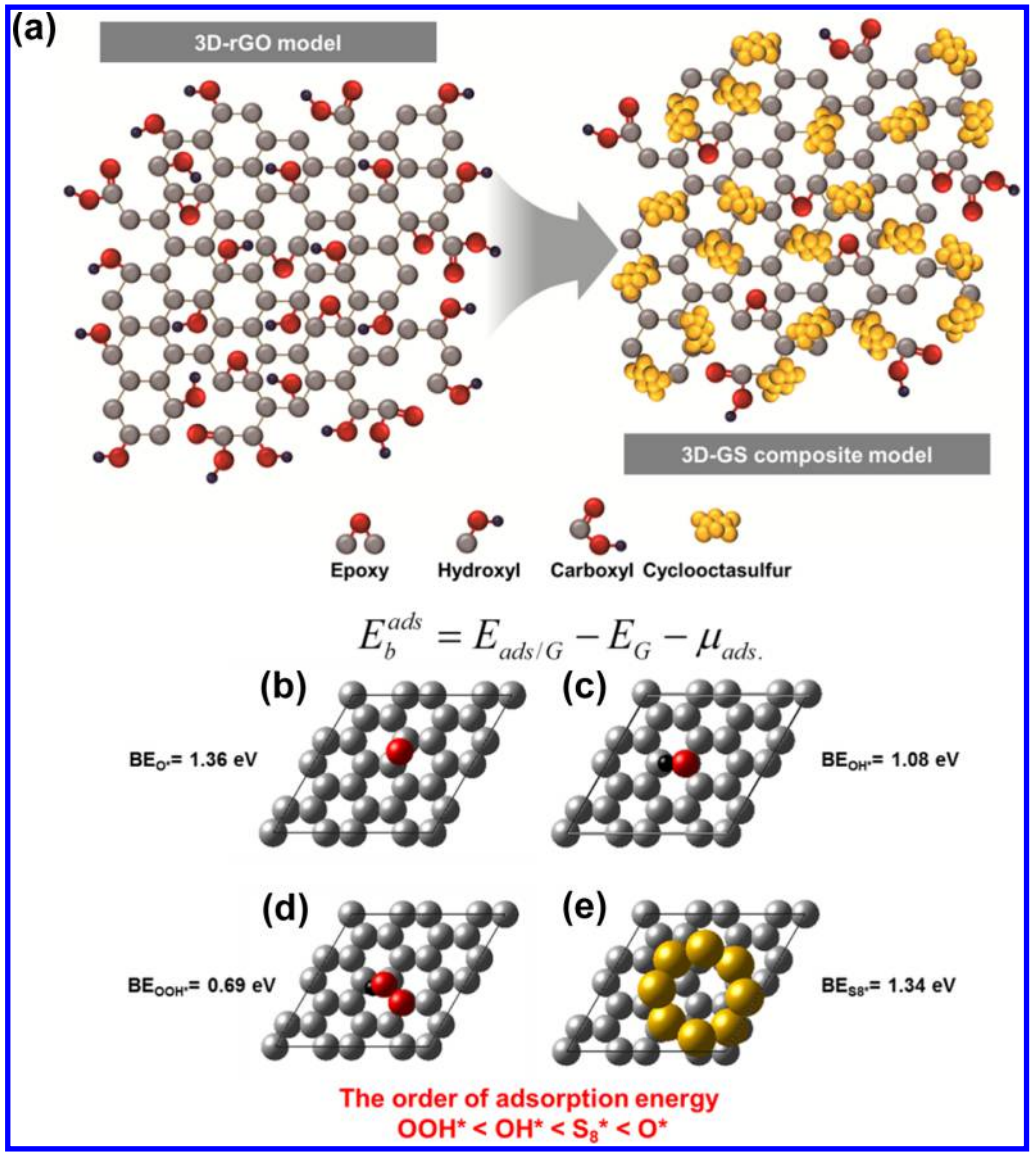

Figure 5. (a) Proposed models of graphene layer which consist of epoxy, hydroxyl and carboxyl groups (−OH, −COOH, and −C−O−C). (b−e) Calculated binding energies of each oxygen functional group. 3D-GS composite most likely forms by replacement of hydroxyl and carboxyl groups by sulfur (S_8).

reported work, respectively.[20,26] Figure 4b displays the XPS results of C 1s of C-GS, M-GS, and 3D-GS, and the area ratio of these samples are presented in Table S3. Each XPS peak shows different characteristic peaks, corresponding to the reference binding energy.[27,28] The XPS result of O 1s further elucidates the type of oxygen functional groups that are consumed during the formation of 3D-GS. Each oxygen functional group is possibly bonded with carbon displayed in Figure 4c, and the area ratio is presented in Table S4.[29,30] The comparable area ratios of C−O, C═O and C−OH bonds of M-GS and C-GS indicate that the contents of oxygen functional groups are similar. However, 3D-GS shows relatively lower C−O and C−OH contents than other sulfur-rGO materials, particularly the C−OH group, which shows lower content than that of 3D-rGO, which is a strong indication that the sulfur has reacted mostly with C−OH during the synthesis which is observed to be still remaining in 3D-rGO above. From this result, it is verified that the dominant interaction between the sulfur and rGO sheets is derived from the substitution reaction between OH and sulfur.

On the basis of the above physical characterization results, the reaction mechanism of the formation of 3D-GS is hypothesized as follows. The rGO constructed from GO-water suspension by an abrupt freezing suppresses agglomeration of graphene sheets in rGO, resulting in a highly aligned three-dimensional sponge structure. It is noted that the sudden freezing is reported to be effective for creating aligned/ordered porous structure and flattened planes of graphene oxide sheets as the frozen water inside the matrix of GO-water suspension helps to maintain the structure by using unidirectional freezing technique.[31−33] The 3D graphene sponge structure then effectively exposes much larger area of graphene surfaces compared to conventional rGO flakes or powders that agglomerate much readily, significantly losing its active surface area. This means that the degree of exposure of the oxygen functional groups such as epoxy, hydroxyl, and carboxyl found in the above XPS analysis of 3D graphene sponge is much larger as well, allowing a higher rate of interaction with sulfur (S_8). This prolific interaction between sulfur and oxygen groups leads to the generation of a nano sulfur granules assembled film

DOI: 10.1021/acsami.5b10267
ACS Appl. Mater. Interfaces 2016, 8, 1984−1991

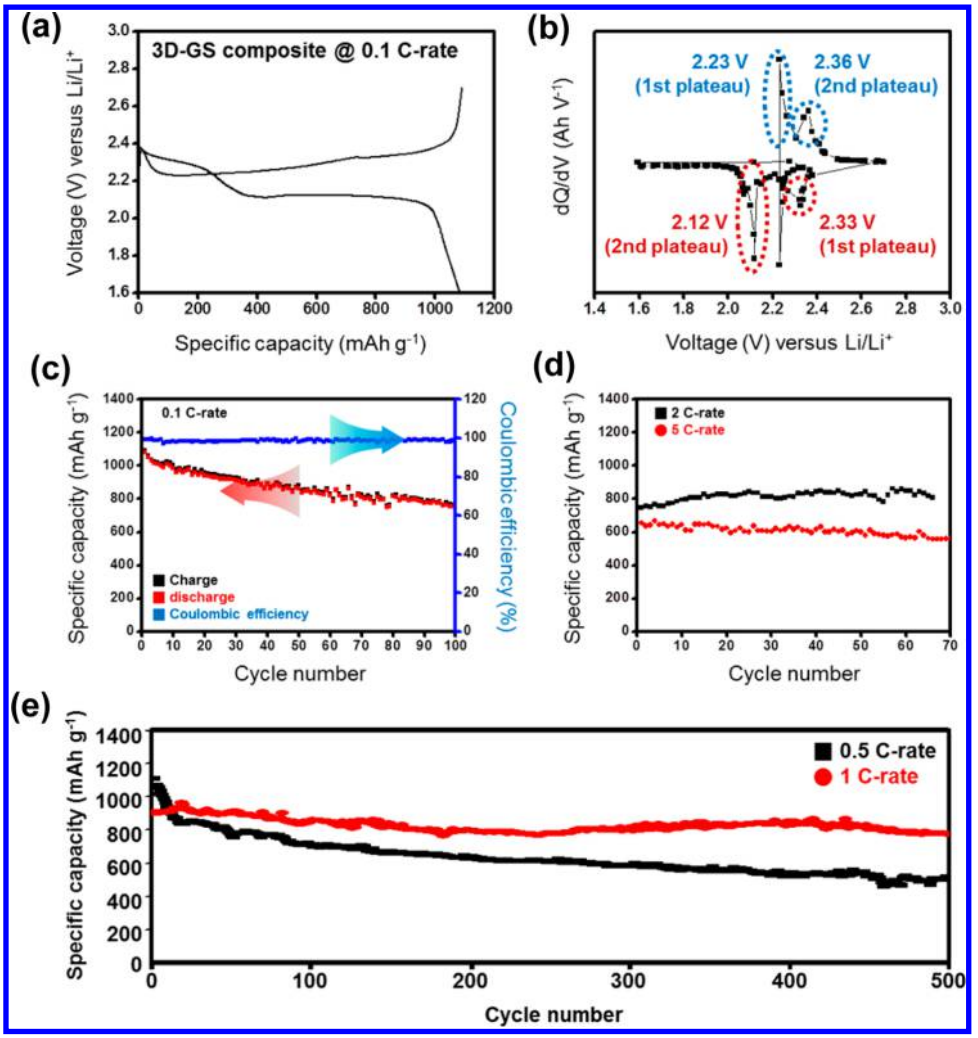

Figure 6. High power lithium sulfur battery performance obtained with 3D-GS composite. (a) Initial charge−discharge profiles of 3D-GS. (b) d*Q*/d*V* curve based on the initial charge−discharge profile. (c) Cycle durability test and the corresponding Coulombic efficiency obtained at 0.1*C* rate. (d) and (e) Cycle durability of 3D-GS composite at various high *C* rates ranging from 0.5 to 5.

laminated on the surface of underlying graphene sheets. In contrast, using powdered graphene would lead to the formation of big size of sulfur particles either dispersed in the graphene matrix or wrapped by graphene layers due to the lack of interaction with oxygen groups, as frequently reported in the literature.[18,21,22] Therefore, the hypothesis for the synthesis of 3D-GS can be summarized as follows: (i) 3D graphene sponge better exposes OH functional groups. (ii) Prolific sulfur interaction with OH group occurs. (iii) Nano granules assembled sulfur film is generated on the graphene surface, as opposed to sulfur particle growth due to the lack of interaction with exposed oxygen groups as in conventional sulfur-graphene composites. In order to support the aforementioned hypothesis of the sulfur film formation on graphene sheets of rGO, DFT modeling calculation has been conducted. The possible model of graphene layer including oxygen functional groups based on literatures[30,34] is presented in Figure 5a, consisting of epoxy, carboxyl and hydroxyl on its surface. Figure 5b−e shows the fully relaxed structures of O, OOH, OH and S_8 adsorbed on the $(2\sqrt{3} \times 2\sqrt{3})$ graphene surface. On the basis of these models, the binding energies (ΔE_{BE}) have been calculated to elucidate the homogeneous layer formation of S_8 on the surface graphene sheets of 3D-rGO sheets as defined by follows eq 1

$$\Delta E_{BE} = E_{ads/G} - E_G - E_{ads.} \quad (1)$$

where $E_{ads/G}$, E_G, and E_{ads} are total energies of graphene surface with adsorbates (e.g., O*, OH*, OOH*, and S_8*), the graphene, and isolated adsorbates in vacuum, respectively. The S_8 and oxygenates functional groups could be absorbed competitively on the surface of graphene during the synthesis. The binding energy is ordered in the sequence of O* > S_8 > OH* > OOH* on graphene. The strongest bond with O corroborates the XPS results for which the specific C═O functional group remains in relatively higher quantity even after 3D-GS synthesis. Furthermore, the binding energy of S_8, which is relatively stronger than OH and OOH, but weaker than O, most likely leads to the replacement of OH and OOH bonds on the graphene surface. Based on previously published results in the literature on rGO, OH, and OOH primarily resides in the in-plane and edges of graphene sheets, respectively.[30,34] This means that the sulfur film formation on graphene sheets observed by SEM and TEM is driven by the replacement of the OH groups by sulfur during the synthesis, consistent with significantly reduced OH content of 3D-GS found in the XPS analysis.

Having created a unique sulfur film morphology and elucidated its synthesis mechanism, the morphological

DOI: 10.1021/acsami.5b10267
ACS Appl. Mater. Interfaces 2016, 8, 1984−1991

advantage of 3D-GS as high performance active material for lithium sulfur battery is demonstrated. Figure 6a, c shows the charge−discharge profile and cyclability of 3D-GS obtained by electrochemical evaluations of the lithium sulfur cell, respectively. Plot of differential capacity (dQ/dV) vs potential (V) reproduced from the first discharge−charge profile is presented in Figure 6b. Two pairs of peaks are observed on the dQ/dV vs V plot at 2.23 and 2.36 V (vs Li/Li^+) during charge, and 2.23 and 2.12 V (vs Li/Li^+) during discharge, respectively. These peaks correspond to the two step reaction, and are typical characteristics of the formation of high-ordered (Li_2S_n, $4 \le n \le 8$), and low-ordered (Li_2S_n, $n < 4$) lithium polysulfides, respectively.[35] As expected, outstanding initial discharge capacity of 1080 mAh g^{-1} (0.91 mAh/cm^2) is obtained with 3D-GS at a 0.1C rate (sulfur mass loading: 0.72−0.74 mg/cm^2, 0.12 mA/cm^2), based on the theoretical capacity of sulfur (1672 mAh g^{-1} S), and the capacity of 763 mAh g^{-1} (with 71% retention even after 100 cycles has been achieved. The Coulombic efficiencies of the initial and 100th cycles are 99.4 and 99.3%, respectively. In comparison, the electrochemical properties of reference materials M-GS and C-GS are presented in Figure S12, where their initial performance are similar to that of 3D-GS, demonstrating 944 and 1126 mAh g^{-1}, (0.78 and 0.92 mAg/cm^2) respectively; however, the capacity retention are significantly lower resulting in 44.7% and 54% only after 50 cycles, respectively. Based on these results, much superior capacity retention of 3D-GS is attributed to the direct connectivity between a homogeneous sulfur film and the graphene sponge, which are absent in a simple sulfur-graphene mixture (M-GS) and sulfur loaded on graphene powder (C-GS). The rate capability of 3D-GS presented in Figure 6e shows the initial capacities of 1015 and 899 mAh g^{-1}, and the capacity retentions of 50.7 and 86.2% (515 and 775 mAh g^{-1}) after 500 cycles obtained at 0.5 and 1.0 C-rate (0.62 and 1.24 mA/cm^2), respectively. The rate capability performance at 2.0 and 5.0 C-rate (2.47 and 6.2 mA/cm^2) is also shown in Figure 6d demonstrating 828 and 599 mAh g^{-1} at 50th cycle with good cycle stability, respectively. The initial capacity decreases with increasing current density due to the polarization-concentration resistance and IR drop of the cell. It is noted that the charge−discharge time of 1.0C rate is twice faster than 0.5C rate during the cell test, which means that the retention time of soluble high-ordered lithium polysulfide (intermediate species) in organic electrolyte at higher C rates is much shorter than lower C rates, leading to higher utilization of sulfur as cycle advances. Despite intrinsically negative properties of sulfur in organic electrolytes, the cyclability of the battery with 3D-GS using higher current densities ranging from 1−5C rate is more stable than 0.1 and 0.5C rate based on the reduced reaction time for the 2 step plateau reaction of solid phase → liquid phase → solid phase ($S_8 \rightarrow Li_2S_{(n-1)}$, $(4 \le n \le 8) \rightarrow Li_2S_n$, $(n \le 2)$ during the charge−discharge process.

CONCLUSIONS

In summary, a homogeneous and uniformly distributed nano granules assembled sulfur-rGO sponge (3D-GS) film composite for lithium sulfur batteries has been successfully synthesized by using carbon disulfide (CS_2) solution method and its electrochemical performance in a lithium−sulfur battery has been investigated. On the bsis of XPS and DFT calculation results, the synthesized sulfur layer, which is deposited on the surface of graphene sheets in rGO sponge, has nano granules assembled, laminated morphology. The reaction mechanism of sulfur film formation on rGO sheets is based on the dominant driving force of sulfur nucleation by consuming specific oxygen functional groups such as −OH and −OOH of rGO. 3D-GS composite exhibits excellent performance with high specific capacity of 1080 mAh g^{-1} at the initial discharge capacity and stable cycle durability even after 100 cycles at 0.1C rate. Furthermore, the initial discharge capacity and capacity retention after 500 cycles at 1.0C rate of 899 mAh g^{-1} and 86.2% have been obtained, respectively. The high initial capacity and cycle durability of 3D-GS is attributed to facile kinetics of the charge-transfer reaction that likely have originated from highly conductive electron paths formed by perfectly connected sulfur film on rGO sheets. On that basis of the enhanced cycle performance, it was concluded that the 3D-GS (sulfur-rGO film) composite is a promising cathode material for rechargeable lithium sulfur batteries and this simple methodology using graphene sponge is highly applicable to new designs for materials science.

ASSOCIATED CONTENT

Supporting Information

The Supporting Information is available free of charge on the ACS Publications website at DOI: 10.1021/acsami.5b10267.

Detailed preparation of samples, characterizations, computational detail, TGA, SEM, TEM, EDX, XRD, Raman spectra, XPS results, and additional electrochemical properties such as cyclic voltammetry, rate capability, cyclability, and EIS (PDF)

AUTHOR INFORMATION

Corresponding Author

*E-mail: zhwchen@uwaterloo.ca.

Author Contributions

Z.C. directed the research. Z.C. and W.A. designed the research. W A., Y.-S.J., and A.Y. conducted synthesis of GO and rGO sponge. M.H.S. conducted DFT computational calculation. W.A. and F.M.H. conducted Raman spectra mapping characterization and discussed on the result. W.A. and D.U.L. conducted all physical characterizations and discussion. W.A. and X.W. conducted electrochemical testing and discussion. W.A. and D.U.L. wrote the paper. All authors extensively discussed the results of the manuscript. All authors have given approval to the final version of the manuscript.

Notes

The authors declare no competing financial interest.

ACKNOWLEDGMENTS

This research was supported by the Natural Sciences and Engineering Research Council of Canada (NSERC) through grants to Z.C. and the University of Waterloo.

ABBREVIATIONS

3D-GO, graphite oxide sponge
3D-rGO, reduced graphene oxide sponge
3D-GS, sulfur nanogranular film coated three-dimensional graphene sponge composite
M-GS, sulfur-graphene mixture
C-GS, sulfur-graphene composite

DOI: 10.1021/acsami.5b10267
ACS Appl. Mater. Interfaces 2016, 8, 1984−1991

REFERENCES

(1) Thackeray, M. M.; Wolverton, C.; Isaacs, E. D. Electrical Energy Storage for Transportation—Approaching the Limits of, and Going Beyond, Lithium-Ion Batteries. *Energy Environ. Sci.* **2012**, *5* (7), 7854−7863.

(2) Sanfélix, J.; Messagie, M.; Omar, N.; Van Mierlo, J.; Hennige, V. Environmental Performance of Advanced Hybrid Energy Storage Systems for Electric Vehicle Applications. *Appl. Energy* **2015**, *137*, 925−930.

(3) Imanishi, N.; Yamamoto, O. Rechargeable Lithium−Air Batteries: Characteristics and Prospects. *Mater. Today* **2014**, *17* (1), 24−30.

(4) Scrosati, B.; Garche, J. Lithium Batteries: Status, Prospects and Future. *J. Power Sources* **2010**, *195* (9), 2419−2430.

(5) Zhou, G.; Paek, E.; Hwang, G. S.; Manthiram, A. Long-life Li/Polysulphide Batteries with High Sulphur Loading Enabled by Lightweight Three-dimensional Nitrogen/Sulphur-codoped Graphene Sponge. *Nat. Commun.* **2015**, *6*, 7760.

(6) Jung, H. G.; Hassoun, J.; Park, J. B.; Sun, Y. K.; Scrosati, B. An Improved High-Performance Lithium-Air Battery. *Nat. Chem.* **2012**, *4* (7), 579−585.

(7) Nelson, J.; Misra, S.; Yang, Y.; Jackson, A.; Liu, Y.; Wang, H.; Dai, H.; Andrews, J. C.; Cui, Y.; Toney, M. F. In Operando X-ray Diffraction and Transmission X-ray Microscopy of Lithium Sulfur Batteries. *J. Am. Chem. Soc.* **2012**, *134* (14), 6337−6343.

(8) Zhou, G.; Pei, S.; Li, L.; Wang, D. W.; Wang, S.; Huang, K.; Yin, L. C.; Li, F.; Cheng, H. M. A Graphene-pure-Sulfur Sandwich Structure for Ultrafast, Long-life Lithium-Sulfur Batteries. *Adv. Mater.* **2014**, *26* (4), 625−631.

(9) Elazari, R.; Salitra, G.; Garsuch, A.; Panchenko, A.; Aurbach, D. Sulfur-Impregnated Activated Carbon Fiber Cloth as a Binder-free Cathode for Rechargeable Li-S Batteries. *Adv. Mater.* **2011**, *23* (47), 5641−5644.

(10) Ji, X.; Evers, S.; Black, R.; Nazar, L. F. Stabilizing Lithium-Sulphur Cathodes Using Polysulphide Reservoirs. *Nat. Commun.* **2011**, *2*, 325.

(11) Wei Seh, Z.; Li, W.; Cha, J. J.; Zheng, G.; Yang, Y.; McDowell, M. T.; Hsu, P. C.; Cui, Y. Sulphur-TiO_2 Yolk-shell Nanoarchitecture with Internal Void Space for Long-cycle Lithium-Sulphur Batteries. *Nat. Commun.* **2013**, *4*, 1331.

(12) Ji, X.; Lee, K. T.; Nazar, L. F. A Highly Ordered Nanostructured Carbon-Sulphur Cathode for Lithium-Sulphur Batteries. *Nat. Mater.* **2009**, *8* (6), 500−506.

(13) Yang, C. P.; Yin, Y. X.; Guo, Y. G.; Wan, L. J. Electrochemical (de)lithiation of 1D Sulfur Chains in Li-S Batteries: A Model System Study. *J. Am. Chem. Soc.* **2015**, *137* (6), 2215−2218.

(14) Zhao, S.; Li, C.; Wang, W.; Zhang, H.; Gao, M.; Xiong, X.; Wang, A.; Yuan, K.; Huang, Y.; Wang, F. A Novel Porous Nanocomposite of Sulfur/Carbon Obtained from Fish Scales for Lithium−Sulfur Batteries. *J. Mater. Chem. A* **2013**, *1* (10), 3334−3339.

(15) Schuster, J.; He, G.; Mandlmeier, B.; Yim, T.; Lee, K. T.; Bein, T.; Nazar, L. F. Spherical Ordered Mesoporous Carbon Nanoparticles with High Porosity for Lithium-Sulfur Batteries. *Angew. Chem., Int. Ed.* **2012**, *51* (15), 3591−3595.

(16) Zu, C.; Su, Y. S.; Fu, Y.; Manthiram, A. Improved Lithium-Sulfur Cells with a Treated Carbon Paper Interlayer. *Phys. Chem. Chem. Phys.* **2013**, *15* (7), 2291−2297.

(17) Ji, L.; Rao, M.; Zheng, H.; Zhang, L.; Li, Y.; Duan, W.; Guo, J.; Cairns, E. J.; Zhang, Y. Graphene Oxide as a Sulfur Immobilizer in High Performance Lithium/Sulfur Cells. *J. Am. Chem. Soc.* **2011**, *133* (46), 18522−18525.

(18) Wang, H.; Yang, Y.; Liang, Y.; Robinson, J. T.; Li, Y.; Jackson, A.; Cui, Y.; Dai, H. Graphene-Wrapped Sulfur Particles as a Rechargeable Lithium-Sulfur Battery Cathode Material with High Capacity and Cycling Stability. *Nano Lett.* **2011**, *11* (7), 2644−2647.

(19) Du, W. C.; Yin, Y. X.; Zeng, X. X.; Shi, J. L.; Zhang, S. F.; Wan, L. J.; Guo, Y. G. Wet Chemistry Synthesis of Multidimensional Nanocarbon-Sulfur Hybrid Materials with Ultrahigh Sulfur Loading for Lithium-Sulfur Batteries. *ACS Appl. Mater. Interfaces* **2015**, DOI: 10.1021/acsami.5b07468.

(20) Zhou, G.; Yin, L.-C.; Wang, D.-W.; Li, L.; Pei, S.; Gentle, I. R.; Li, F.; Cheng, H.-M. Fibrous Hybrid of Graphene and Sulfur Nanocrystals for High-Performance Lithium−Sulfur Batteries. *ACS Nano* **2013**, *7* (6), 5367−5375.

(21) Zu, C.; Manthiram, A. Hydroxylated Graphene-Sulfur Nanocomposites for High-Rate Lithium-Sulfur Batteries. *Adv. Energy Mater.* **2013**, *3* (8), 1008−1012.

(22) Xi, K.; Kidambi, P. R.; Chen, R.; Gao, C.; Peng, X.; Ducati, C.; Hofmann, S.; Kumar, R. V. Binder Free Three-dimensional Sulphur/few-Layer Graphene Foam Cathode with Enhanced High-rate Capability for Rechargeable Lithium Sulphur Batteries. *Nanoscale* **2014**, *6* (11), 5746−5753.

(23) Wang, C.; Su, K.; Wan, W.; Guo, H.; Zhou, H.; Chen, J.; Zhang, X.; Huang, Y. High Sulfur Loading Composite Wrapped by 3D Nitrogen-doped Graphene as a Cathode Material for Lithium−Sulfur Batteries. *J. Mater. Chem. A* **2014**, *2* (14), 5018−5023.

(24) Ahn, W.; Lim, S. N.; Lee, D. U.; Kim, K.-B.; Chen, Z.; Yeon, S.-H. Interaction Mechanism Between a Functionalized Protective Layer and Dissolved Polysulfide for Extended Cycle Life of Lithium Sulfur Batteries. *J. Mater. Chem. A* **2015**, *3* (18), 9461−9467.

(25) Kudin, K. N.; Ozbas, B.; Schniepp, H. C.; Prud'Homme, R. K.; Aksay, I. A.; Car, R. Raman Spectra of Graphite Oxide and Functionalized Graphene Sheets. *Nano Lett.* **2008**, *8* (1), 36−41.

(26) Fu, Y.; Manthiram, A. Orthorhombic Bipyramidal Sulfur Coated with Polypyrrole Nanolayers as a Cathode Material for Lithium−Sulfur Batteries. *J. Phys. Chem. C* **2012**, *116* (16), 8910−8915.

(27) Yumitori, S. Correlation of C1s Chemical State Intensities with the O1s Intensity in the XPS Analysis of Anodically Oxidized Glass-like Carbon Samples. *J. Mater. Sci.* **2000**, *35* (1), 139−146.

(28) Chiang, T.; Seitz, F. Photoemission Spectroscopy in Solids. *Ann. Phys. (Berlin, Ger.)* **2001**, *10*, 61−74.

(29) Ahn, W.; Song, H. S.; Park, S.-H.; Kim, K.-B.; Shin, K.-H.; Lim, S. N.; Yeon, S.-H. Morphology-Controlled Graphene Nanosheets as Anode Material for Lithium-Ion Batteries. *Electrochim. Acta* **2014**, *132*, 172−179.

(30) Yang, D.; Velamakanni, A.; Bozoklu, G.; Park, S.; Stoller, M.; Piner, R. D.; Stankovich, S.; Jung, I.; Field, D. A.; Ventrice, C. A. Chemical Analysis of Graphene Oxide Films after Heat and Chemical Treatments by X-ray Photoelectron and Micro-Raman Spectroscopy. *Carbon* **2009**, *47* (1), 145−152.

(31) Peppin, S. S. L.; Wettlaufer, J. S.; Worster, M. G. Experimental Verification of Morphological Instability in Freezing Aqueous Colloidal Suspensions. *Phys. Rev. Lett.* **2008**, *100* (23), 238301.

(32) Kwon, S.-M.; Kim, H.-S.; Jin, H.-J. Multiwalled Carbon Nanotube Cryogels with Aligned and Non-aligned Porous Structures. *Polymer* **2009**, *50* (13), 2786−2792.

(33) Nakagawa, K.; Yasumura, Y.; Thongprachan, N.; Sano, N. Freeze-dried Solid Foams Prepared from Carbon Nanotube Aqueous Suspension: Application to Gas Diffusion Layers of a Proton Exchange Membrane Fuel Cell. *Chem. Eng. Process.* **2011**, *50* (1), 22−30.

(34) Dreyer, D. R.; Park, S.; Bielawski, C. W.; Ruoff, R. S. The Chemistry of Graphene Oxide. *Chem. Soc. Rev.* **2010**, *39* (1), 228−240.

(35) Ahn, W.; Kim, K.-B.; Jung, K.-N.; Shin, K.-H.; Jin, C.-S. Synthesis and Electrochemical Properties of a Sulfur-Multi Walled Carbon Nanotubes Composite as a Cathode Material for Lithium Sulfur Batteries. *J. Power Sources* **2012**, *202*, 394−399.

DOI: 10.1021/acsami.5b10267
ACS Appl. Mater. Interfaces 2016, 8, 1984−1991